Solar-like oscillations with low amplitude in the CoRoT[⋆] target HD 181906

R. A. García[1], C. Régulo[2,3], R. Samadi[4], J. Ballot[5], C. Barban[4], O. Benomar[6], W.J. Chaplin[7], P. Gaulme[6], T. Appourchaux[6], S. Mathur[8], B. Mosser[4], T. Toutain[7], G. A. Verner[9], M. Auvergne[4], A. Baglin[4], F. Baudin[6], P. Boumier[6], H. Bruntt[4,10], C. Catala[4], S. Deheuvels[4], Y. Elsworth[7], S.J. Jiménez-Reyes[2], E. Michel[4], F. Pérez Hernández[2,3], I. W. Roxburgh[9,4], and D. Salabert[2]

[1] Laboratoire AIM, CEA/DSM-CNRS-Université Paris Diderot; CEA, IRFU, SAp, centre de Saclay, F-91191, Gif-sur-Yvette, France e-mail: Rafael.Garcia@cea.fr
[2] Instituto de Astrofísica de Canarias, 38205, La Laguna, Tenerife, Spain
[3] Universidad de La Laguna, 38206 La Laguna, Tenerife, Spain
[4] LESIA, UMR8109, Université Pierre et Marie Curie, Université Denis Diderot, Obs. de Paris, 92195 Meudon Cedex, France
[5] Laboratoire d'Astrophysique de Toulouse-Tarbes, Université de Toulouse, CNRS, 14 av. Edouard Belin, F-31400 Toulouse, France
[6] Institut d'Astrophysique Spatiale, UMR8617, Université Paris XI, Batiment 121, 91405 Orsay Cedex, France
[7] School of Physics and Astronomy, University of Birmingham, Edgbaston, Birmingham B15 2TT, UK
[8] Indian Institute of Astrophysics, Bangalore, India
[9] Astronomy Unit, Queen Mary, University of London Mile End Road, London E1 4NS, UK5
[10] Sydney Institute for Astronomy, School of Physics, The University of Sydney, NSW 2006, Australia

ABSTRACT

Context. The F8 star HD 181906 (effective temperature ∼ 6300 K) was observed for 156 days by the CoRoT satellite during the first long run in the centre direction. Analysis of the data reveals a spectrum of solar-like acoustic oscillations. However, the faintness of the target (m_v=7.65) means the signal-to-noise (S/N) in the acoustic modes is quite low, and this low S/N leads to complications in the analysis.
Aims. To extract global variables of the star as well as key parameters of the p modes observed in the power spectrum of the lightcurve.
Methods. The power spectrum of the lightcurve, a wavelet transform and spot fitting have been used to obtain the average rotation rate of the star and its inclination angle. Then, the autocorrelation of the power spectrum and the power spectrum of the power spectrum were used to properly determine the large separation. Finally, estimations of the mode parameters have been done by maximizing the likelihood of a global fit, where several modes were fit simultaneously.
Results. We have been able to infer the mean surface rotation rate of the star (∼4 μHz) with indications of the presence of surface differential rotation, the large separation of the p modes (∼87 μHz), and therefore also the "ridges" corresponding to overtones of the acoustic modes.

Key words. methods: statistical – methods: observational – stars: oscillations – stars: individual: HD 181906

1. Introduction

CoRoT (Convection, Rotation and planetary Transits) is a minisatellite launched on December 26, 2006 and developed by the French Space agency CNES (Centre National d'Etudes Spatiales) in collaboration with the Science Programmes of ESA (European Space Agency), Austria, Belgium, Brazil, Germany and Spain. The main objectives are to detect exoplanets and to probe the interiors of stars using asteroseismology (Baglin et al. 2006). The high-perfomance photometric data offer an unprecedented opportunity to detect extremely low amplitude oscillations in many stars (Michel et al. 2008b), in particular, in solar-like oscillating stars. The main programme of the CoRoT mission consists of 5-month-long runs during which ten designated targets are almost continuously monitored with a 32-s cadence for seismic studies. Several solar-like oscillation stars have al-

ready been observed with CoRoT (García et al. 2008). One of them is HD 181906, a faint F8 star which has been observed during the first long run looking into the galactic centre direction at the same time as HD 181420 (Barban et al. 2009).

In the present paper we report the first detailed seismic analysis of HD 181906 using CoRoT data. We first present some classical characteristics of the star and infer some expected pulsation properties in Sect. 2; after a description of the CoRoT observations (Sect. 3), we derive the surface rotation of the star (Sect. 4), we then determine the region where the p modes are (Sect. 5) and we explain how to take into account the convective background (Sect. 6). We finish by analysing the p-mode spectrum (Sect. 7) and extracting the p-mode parameters (Sect.8).

2. Stellar parameters and estimated oscillation properties

The star HD 181906 (or HIP 95221) is known as an F8 dwarf with a magnitude m_v = 7.65 and is probably a binary system as suggested by astrometric measurements (Makarov & Kaplan

---

2005; Frankowski et al. 2007) or high-resolution spectroscopy (Bruntt 2009). The new reduction of Hipparcos data by van Leeuwen (2007) provides a parallax $\pi = 14.72 \pm 0.91$ mas (i.e. a distance $d = 68 \pm 4$ pc), which leads to an absolute magnitude of $M_V = 3.49 \pm 0.13$. Using $BC_V = -0.044 \pm 0.058$ for the bolometric correction in the V band (Masana et al. 2006), we deduce the stellar luminosity $L = 3.32 \pm 0.45\,L_\odot$. Very recently Bruntt (2009) has derived global parameters for this star from high-resolution spectroscopy. He found a value of $T_{\rm eff} = 6300 \pm 150$ K which is in perfect agreement with the value he derived from 2MASS photometry ($T_{\rm eff} = 6360 \pm 100$ K). He also deduced a surface gravity $\log g = 4.220 \pm 0.056$ and a metallicity [Fe/H] $= -0.11 \pm 0.14$. Using his observations as inputs for stellar modelling, he estimated for this star a mass $M = 1.144 \pm 0.119\,M_\odot$, a radius $R = 1.392 \pm 0.054\,R_\odot$ and an age of 4.2 ± 1.6 Gyr. These values have been hereafter used to approximate seismic quantities and are summarized Table 1.

Table 1. Global parameters of HD 181906 used for this work.

π	14.72 ± 0.91 mas
$L/L_\odot$	3.32 ± 0.45
$T_{\rm eff}$	6300 ± 150 K
$\log g$	4.220 ± 0.056
[Fe/H]	-0.11 ± 0.14 dex
$v \sin i$	10 ± 1 km s^{-1}
$M/M_\odot$	1.144 ± 0.119
$R/R_\odot$	1.392 ± 0.054

We have compared these values to those derived in previous works using differents techniques. This star is included in the Geneva-Copenhagen survey of the Solar neighbourhood (Nordström et al. (2004) revisited by Holmberg et al. (2007)). This survey, mainly based on Strömgren photometry, provides an effective temperature $T_{\rm eff} = 6382 \pm 91$ K and metallicity [Fe/H] $= -0.18 \pm 0.10$ dex. The age is also estimated to $2.7^{+0.3}_{-0.4}$ Gyr and the mass to $1.22^{+0.06}_{-0.07}\,M_\odot$. All of these values are in very good agreement with those of Bruntt (2009). By using V and 2MASS IR photometry, Masana et al. (2006) recover a slightly higher effective temperature of 6532 ± 66 K and provide an angular semi-diameter SD $= 0.102 \pm 0.001$ mas. Thus, using the new Hipparcos parallax, we estimate the stellar radius to $1.50 \pm 0.10\,R_\odot$[1], which is consistent with Bruntt (2009).

For the the rotation velocity, Nordström et al. (2004) have reported a measurement based on earlier CORAVEL observations and have estimated the rotation velocity $v \sin i \approx 16 \pm 1$ km s^{-1}. However, according to Bruntt (2009), this value is overestimated due to the blend with a second star. By taking into account the presence of this second star, $v \sin i$ decreases to 10 ± 1 km s^{-1}. For consistency reasons, we have considered the latter.

Using these parameters, we are able to obtain approximate values of some global seismic parameters using scaling laws. The large separation, $\Delta \nu$, can be estimated from the mass and the radius as follows (Kjeldsen & Bedding 1995):

$$\Delta \nu = \left(\frac{M}{M_\odot}\right)^{1/2} \cdot \left(\frac{R}{R_\odot}\right)^{-3/2} \cdot 135\,\mu\text{Hz} . \qquad (1)$$

A value of $\Delta \nu \approx 88 \pm 7\,\mu$Hz has been obtained.

---

[1] this number is 5% lower that the one derived by Masana et al. (2006), since the parallax has been revised, but is fully compatible within the error bar.

The frequency of the maximum of the p modes scales as the cut-off frequency (Kjeldsen & Bedding 1995). This law has lately been verified using spectrometric data (Bedding & Kjeldsen 2003). Therefore we can express ν_{max} as follows:

$$\nu_{max} = \frac{M/M_\odot}{(R/R_\odot)^2 \cdot \sqrt{\frac{T_{\rm eff}}{5777}}} \cdot 3050\,\mu\text{Hz} . \qquad (2)$$

We obtain $\nu_{max} \approx 1725 \pm 225\,\mu$Hz

Finally, the maximum expected amplitude (an estimate of the intrinsic mode amplitude in terms of bolometric intensity fluctuations) can be deduced from Samadi et al. (2007b):

$$A_{max} = \left(\frac{dL}{L}\right)_{max} = \left(\frac{L/L_\odot}{M/M_\odot}\right)^{0.7} \cdot \sqrt{\frac{5777}{T_{\rm eff}}} \cdot A_{\odot\,max} \qquad (3)$$

where we have changed the solar value of $A_{\odot\,max} = 2.6$ ppm to 2.53 ± 0.11 ppm obtained by calibrating different helioseismic measurements of the VIRGO/SoHO package (POM6 & SPM) (Michel et al. 2009). This gives a value of $A_{max} \approx 5.1 \pm 0.6$ ppm for HD 181906. This relation is the combination of two different ones: the adiabatic relation proposed by Kjeldsen & Bedding (1995) to relate mode amplitudes in intensity to mode amplitudes in velocity and the scaling law proposed by Samadi et al. (2007b) which gives the mode amplitudes in velocity as a function of (L/M).

3. CoRoT Observations

156.6 days of continuous data – from 2007 May 11 until 2007 October 15 – have been collected with an overall duty cycle of 89.3 %. Most of the gaps (each of a few minutes duration) are due to data loss during the crossings of the South Atlantic Anomaly (see for a detailed explanation: Auvergne et al. 2009). These gaps have been linearly interpolated in the light curve to avoid putting zeros. We have verified that this interpolation does not introduce any spurious frequencies in the Fourier domain. The original 1-s cadence raw data have been corrected and calibrated into level-2 (or N2) data following the methods described in Samadi et al. (2007a). The N2 light curve is sampled on a regular grid in the heliocentric frame with a cadence of 32s. Then we have removed a low-frequency trend due to the aging of the CCD (Auvergne et al. 2009), and finally we have removed some outlier points (0.013%). The resultant lightcurve shows a small modulation during the first 60 days (see Fig. 1) and then a very flat behavior. At this point, it is not possible to disentangle a real modulation of the star from an instrumental effect. A second modulation – of around 3 days – is also visible and could be related to the surface rotation due to the signature of magnetic activity on the surface of the star.

To compute the power spectrum density (PSD) we have used a standard Fast Fourier Transform algorithm and normalized it as the so-called one-sided power spectral density (Press et al. 1992). The resultant PSD is shown in Fig. 2.

In the PSD, several peaks rise above the general trend dominated by the photon noise from the Nyquist frequency down to approximately $100\,\mu$Hz, and by the convective noise from this frequency until $\sim 10\,\mu$Hz (Michel et al. 2008a). Below this, the spectrum is dominated by two peaks, at around 4 and 8 μHz, that could be the signature of the surface rotation of the star – already seen in its lightcurve – as well as its first harmonic (red dotted lines in Fig 2). We will discuss in detail this rotation rate in the
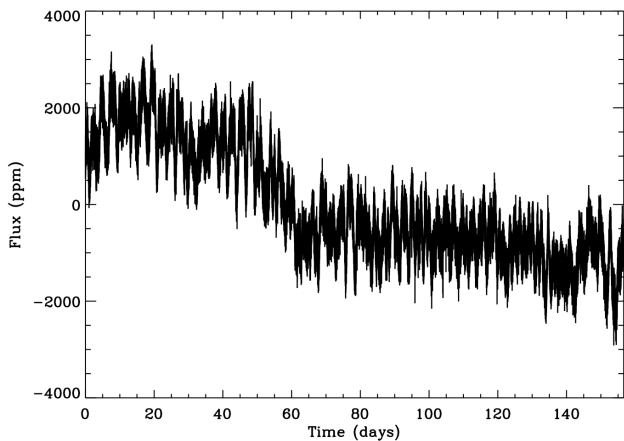
Fig. 1. N2-Light curve (in ppm) corrected for the aging of the CCD and interpolated onto a regular grid in the heliocentric frame.
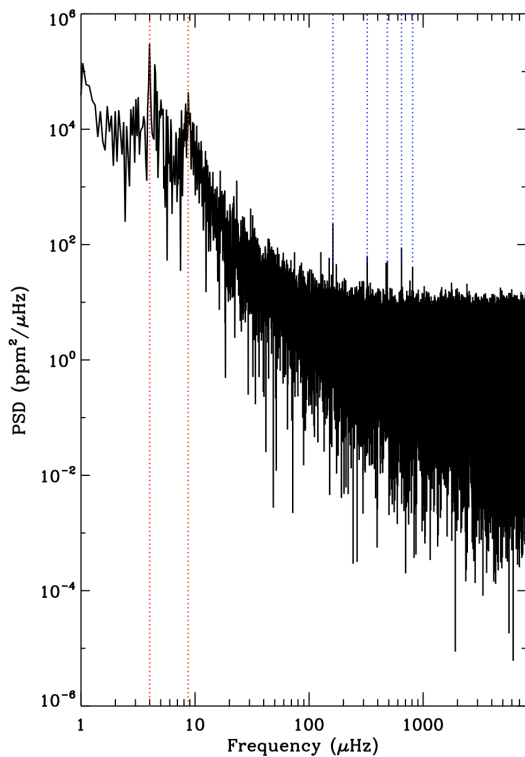

Fig. 2. Power spectrum density of the full 156-day N2-light curve shown in Fig 1. The two red-dotted vertical lines show the lowest significant peak and the first harmonic that could be the signature of the surface rotation of the star. The five blue-dotted vertical lines indicate the first harmonics of the orbital period of the satellite.

next section. The signature of the CoRoT orbital periodicity produces a peak at 161.7 μHz together with several harmonics (blue dotted lines in Fig. 2).

The combination of a lower-than-expected signal-to-noise ratio of the oscillation amplitudes (Michel et al. 2008a) with the faintness of the target (m_v=7.65) means that the p-mode hump is not clearly visible in Fig. 2, but there is a small excess in power

around ~2000 μHz. A more sophisticated treatment is necessary to clearly unveil the acoustic spectrum of this star.

4. Surface rotation

As we have already mentioned in previous sections, the light curve of HD 181906 shows a periodic modulation of about 3 days that produces two peaks in the PSD. It is interesting to analyse this periodicity in a more detailed way.

We have started by calculating a time-period diagram using wavelets (Torrence & Compo 1998). The advantage of this technique relies on the fact that we use a wave, the Morlet wavelet – a sine wave modulated by a Gaussian (Goupillaud et al. 1984) – which has a finite duration and a specific frequency. By changing the frequency of this wavelet and sliding it along our time series, we calculate the correlation between the wavelet and the data. That enables us to compute the Wavelet Power Spectrum (see Fig. 3). Most of the power is concentrated along a horizontal line centered at ~ 2.8 days. This signal appears to be stronger during the first half of the run than during the second period.
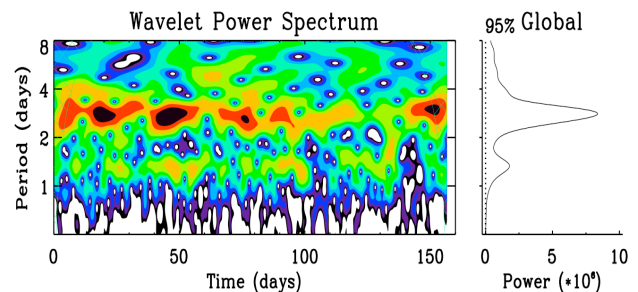

Fig. 3. Left: Wavelet power spectrum for HD 181906 at low frequency. Right: Global Wavelet Power Spectrum where the dotted-line represents the 95% confidence level.

With the Global Wavelet Power Spectrum defined as the horizontal average of the time-period diagram (see Fig. 3 *(right)*), we observe that most of the power – more than 99% – is concentrated in this main periodicity at 2.81 days. A smaller peak is also visible at 1.41 days but containing much less power. This method (successfully tested with numerical simulations and with solar data from the GOLF instrument (Mathur et al. 2008)) allows us to disentangle between the peak corresponding to the main periodicity and that of the harmonic by the simple visual inspection of the PSD where 2 peaks of similar characteristics stand at 4.04 and 8.2 μHz.

A closer inspection of the rotation period, P_{rot}, in the PSD reveals that it is composed of a double structure, with a strong peak centered at 4 μHz – 2.9 days (Fig. 4) – and a smaller one at 4.45 μHz (2.6 days). The fact of having these two peaks instead of just one may suggest the presence of spots at different latitudes with a differential surface rotation. The spot modeling done by Mosser et al. (2009a) states this point explicitly, indicating two rotation periods associated with a clear gradient of the rotational velocity as a function of spot latitude. Another explanation, less probable, is the presence of a hot star in the background of HD 181906, as suggested by Bruntt (2009) who proposed a detailed analysis of the fundamental parameters of CoRoT asteroseismic targets based on high-resolution spectrometric measurements.

If the 156-day time series is divided into two segments of 78 days, or into three independent 52-day subsets, a slightly dif-
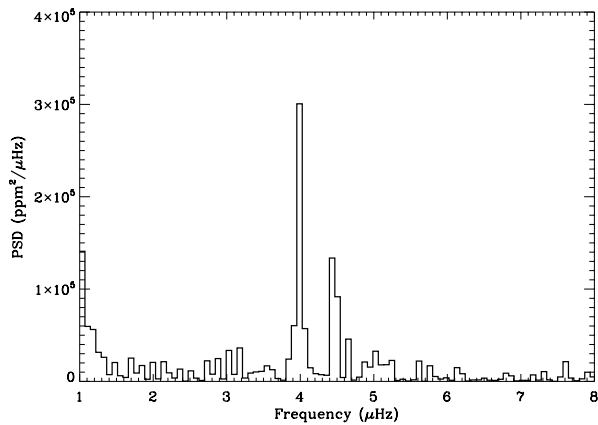
Fig. 4. Zoom on the spectrum at low frequency. The power spectrum density has been computed using the total length of data.

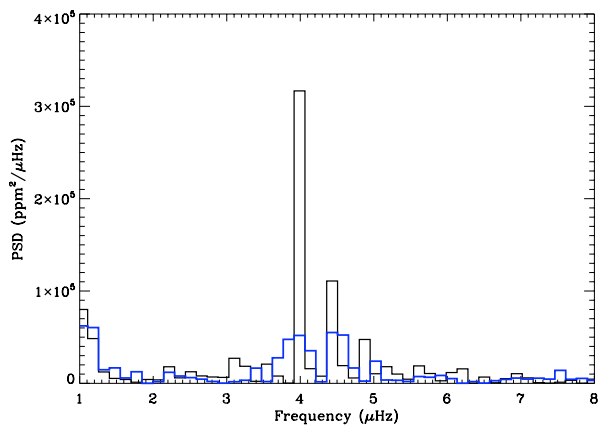ferent low-frequency structure is observed each time, as can be seen in Fig. 5 and Fig. 6.

Fig. 5. Zoom on the spectrum at low frequency. In black the Fourier spectrum of the first 78 days of data. In blue the spectrum of the last 78 days.
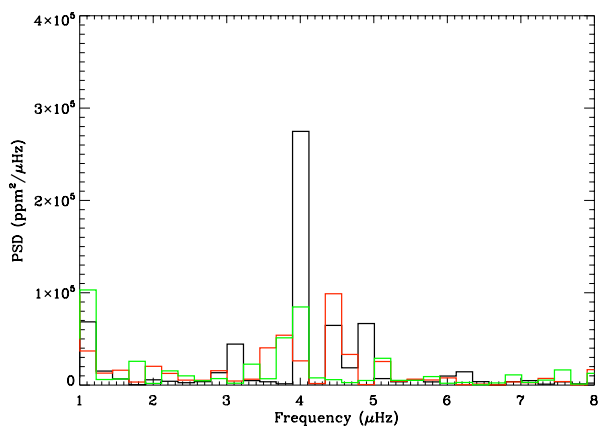

Fig. 6. Zoom on the spectrum at low frequency. In black the Fourier spectrum of the first 52 days of data. In red the spectrum of the 52 intermediate days of data, and in green the spectrum of the last 52 days.

Table 2. Length of spectra and corresponding rotational periods.

Spectrum	μHz (days)	μHz (days)	μHz (days)
Total spectrum	4.00 (2.9)	4.45 (2.6)	–
First 78 days	4.00 (2.9)	4.45 (2.6)	4.90 (2.4)
Second 78 days	4.00 (2.9)	4.58 (2.5)	5.04 (2.4)
First 52 days	4.00 (2.9)	4.45 (2.6)	4.90 (2.4)
Second 52 days	3.77 (3.1)	4.45 (2.6)	–
Third 52 days	4.00 (2.9)	–	5.12 (2.3)

In Fig. 5, the PSD of the first 78 days is plotted in black, and the PSD of the last 78 days is plotted in blue. In Fig. 6, the PSD of the first 52 days is plotted in black, the next 52 days is plotted in red, and the last 52-day segment is plotted in green. Details of the prominent peaks that appear in each of these spectra are summarized in Table 2. In this table, we listed the frequencies (in μHz) and the respective rotational periods (in days) of the peaks that appear at low frequency in the Fourier spectrum of the full-length series and the smaller subseries that we have considered in the analysis. The peaks are located at rotational periods in the range from 2.3 to 3.1 days. The different behavior of the peaks (in frequency and amplitude) – behavior that depends on the observed period – suggests that they could be the signatures of differential rotation on the surface of the star, and not the rotation period of the secondary star in the binary system (which would be expected to produce a stable peak in all the considered periods). Therefore, HD 181906 shows a slightly larger differential rotation than the Sun, but of the same order of magnitude. A more detailed analysis of this behavior will be the topic of a future work.

4.1. Constraining the inclination angle

The angle of inclination of HD 181906 can be inferred from the measured value of $(v \sin i)_{obs}$ and the surface rotation that we have just derived:

$$\sin i = \frac{(v \sin i)_{obs}}{2\pi R \nu_{rot}} \ . \tag{4}$$

Using a rotation frequency of $\nu_{rot} = 4.0 \pm 0.15 \ \mu$Hz and a rotation velocity of $(v \sin i)_{obs} = 10 \pm 1 \ \mathrm{km \, s^{-1}}$ we obtain an angle of $i = 24 \pm 3°$. We recall this value is obtained by taking into account the blend with a second star (Bruntt 2009). For comparison, by considering the older value of $16 \pm 1 \ \mathrm{km \, s^{-1}}$, we would obtain an angle of $37.5 \pm 4.5°$. From the spot modeling (Mosser et al. 2009a) a value of $45 \pm 10°$ has been found. This parameter is extremely important because it affects the amplitude ratios of the components of a multiplet of non-radial modes and it is strongly connected to the rotational splitting (see, for example, Ballot et al. 2008, and references therein).

5. Finding the p-mode region

To find the region where the p modes are centered, we computed the Power Spectrum of the Power Spectrum (PSPS) (or the auto-correlation of the PSD) in the region determined by the scaling laws (see Fig 7 and a more detailed explanation in Sect 7.2).

This revealed a strong peak at half the large separation, $\Delta\nu/2$, with the location of the peak implying $\Delta\nu \sim 87 \ \mu$Hz, which is close to the upper limit of the value estimated in Section 2, using existing, non-seismic data on the star. In order to narrow
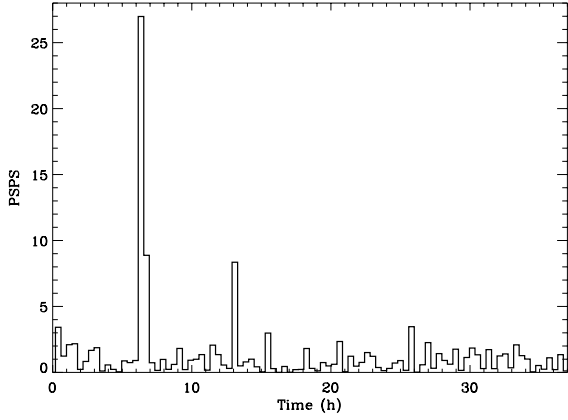
Fig. 7. Power Spectrum of the Power Spectrum (PSPS) normalized by its standard deviation in the region between 1400 and 2100 μHz. The highest peak corresponds to 6.35 hours, i.e. $\Delta\nu$=87.5 $\pm$ 2.6 μHz.

down the range more carefully, we then performed the following procedure.

We moved a 300-μHz-wide window through the frequency range of interest, and computed the PSPS at each location. The window was shifted in steps of 33 μHz. We measured in each PSPS the height of the peak at $\Delta\nu/2$ relative to the local background level. The noise distribution in each PSPS will follow χ^2 two-degrees-of-freedom statistics; given this known distribution, it is possible to calculate a false-alarm probability for the $\Delta\nu/2$ peak to appear by chance (as part of the background) anywhere in the PSPS. We calculated the level corresponding to a 5% of probability of appearing by chance (Chaplin et al. 2002).

The maximum relative height of the $\Delta\nu/2$ peak (i.e., the height divided by the measured background in the PSPS) is plotted in Fig. 8. We find here that the p-mode power is prominent between 1400 and 2100 μHz.
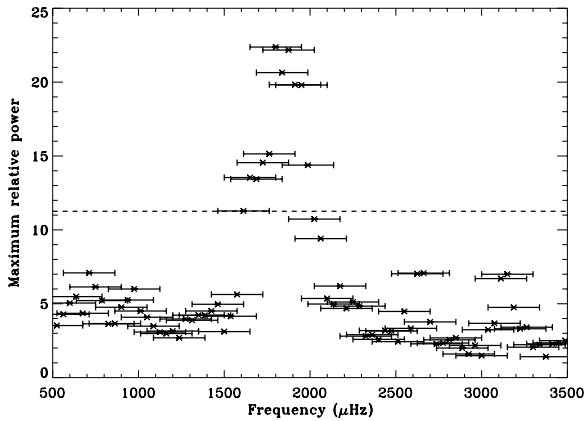

Fig. 8. Maximum of the PSPS in a region around the expected half-large separation computed in 300 μHz-wide windows shifted every 33 μHz. The horizontal error bars show the range in frequency in the PS that was analyzed (300 μHz). The dashed line represents the 95% confidence level.

6. Background fitting

In order to estimate the non-p-mode background, we fit the following three-component model to those parts of the PSD where the observed p-mode power is insignificant (PSD$_{\text{BG}}$):

$$\text{PSD}_{\text{BG}}(\nu) = \left(\sum_{i=1}^{2} \frac{A_i}{1 + (\nu B_i)^{C_i}} \right) + D \qquad (5)$$

There are two power-law components in the summation: a component to represent the significant power at very low frequencies from surface activity; and a component to represent power from surface granulation. Both power-law components are modelled in terms of three parameters: a power spectral density, A; a characteristic timescale, B; and a power-law index, C. The third component in Equation 5, D, models the contribution from shot noise.

Rather than fit the raw power spectrum, we fitted a smoothed spectrum generated by applying an N_s-bin-wide boxcar, taking the independent averages only. With $N_s \gtrsim 30$, independent N_s-bin averages show normally-distributed scatter about the (underlying) limit spectrum we seek to estimate from the fit. A standard least-squares fitting was therefore applied, with weights fixed by the uncertainties on each independent N_s-bin average. These uncertainties were each given by $s/\sqrt{N_s}$, where s is the standard deviation of the N_s contributing power values.

The alternative approach is to fit the raw spectrum by maximizing a likelihood function commensurate with the χ^2 two-degrees-of-freedom statistics. It turns out that the smoothed spectrum may also be fitted by applying the same maximum likelihood estimator (as was shown by (Appourchaux 2004)). These approaches are, however, more sensitive to the choice of initial first-guess parameters than is the least-squares fitting approach applied here, and can as such be prone to poor convergence.

There are a total of seven free parameters defining the background model in Equation 5. We did not, however, fit them all simultanously: some parameters were fixed, as we now go on to explain.

We assumed power in the very low-frequency activity component arises predominantly from the exponential decay of active regions and plage. This decay implies a limiting power density spectrum that is Lorentzian, hence we fixed the activity-component index to a value $C_1 = 2$ during fitting.

Exercises performed with the asteroFLAG artificial asteroseismology data (Chaplin et al. 2008) showed that attempts to fit A_1 and B_1 simultaneously with the other parameters could lead to instability in the procedure and poor convergence. We found that we could stabilize the fitting by fixing A_1 at the value of the power spectral density of the first element of the averaged spectrum, leaving B_1 as the only parameter of the activity component to be fitted. This approach does mean that some care is needed in interpreting the best-fitting value of B_1, since the value for A_1 can be affected by the appearence in the power spectrum of narrow-band features arising from rotational modulation, which are not modelled in Equation 5. The aforementioned approach to the fitting does however give a good representation of the power from the active-region decay that leaks into the frequency region where the granulation is important; which in turn means we can in principle have more confidence in the accuracy of the best-fitting granulation parameters.

7. The p-mode spectrum

Figure 9 plots the PSD of the full-length lightcurve smoothed with a boxcar of 70 points (~ 5.2 μHz). A clear excess of power
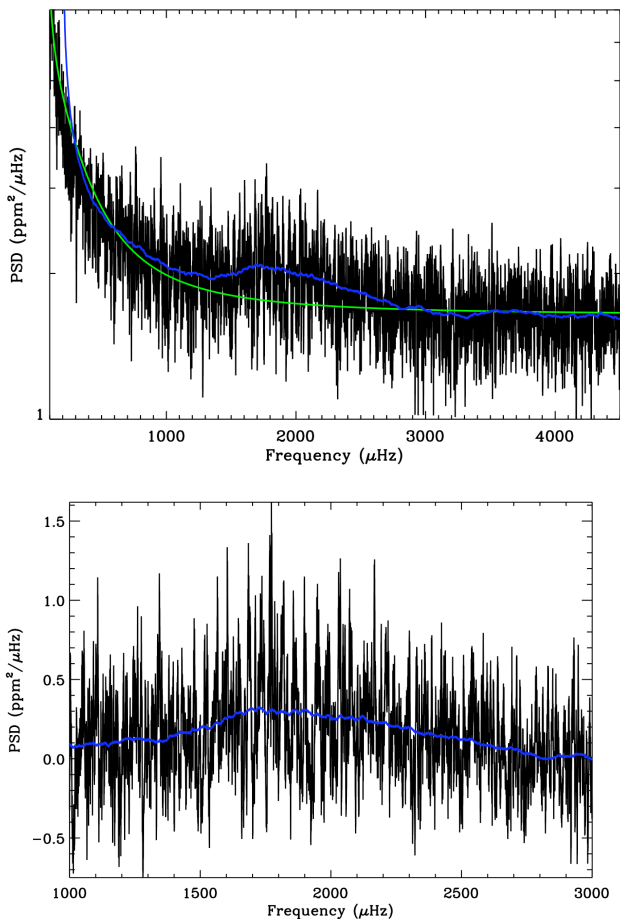
Fig. 9. Power spectrum density of the full length light curve smoothed by a boxcar of 70 points (Top). The continuous green curve is the background fitted using the method explained in Section 6. The bottom panel shows a closer region of the p-mode band between 1000 and 3000 μHz after subtracting the background (green curve in the top panel). The blue curve in both panels is the PSD but smoothed using a boxcar of 5000 points.

Fig. 10. Echelle diagram of the full PSD smoothed by a 70 points boxcar starting at a frequency of 792.5 μHz and using a folding frequency of 87.5 μHz.

is observed, relative to the best-fitting background model (green curve), in the region where the p-mode excess was detected (see Sect. 5). To visually enhance the excess we also show in blue a heavily smoothed spectrum computed by applying a 5000-point boxcar ($\sim 370\,\mu$Hz) to the raw spectrum.

Figure 10 shows the Echelle diagram (Grec et al. 1983) of the 70-point-boxcar smoothed PSD. The diagram covers the frequency region from 792.5 to 3000 μHz, with each horizontal strip covering 87.5 μHz of the spectrum (see Fig. 7). Two ridges appear in the diagram, corresponding to the odd and even modes. Inspection of the diagram shows that it is not possible to discriminate visually between the two ridges, hence the angular-degree tagging is uncertain.

7.1. Global amplitude

The procedure for measuring the mode amplitudes begins by averaging the power spectral density in independent frequency slices of $q\Delta\nu$, where $q = 1$ or 2, and $\Delta\nu$ is the estimated large frequency spacing of the acoustic mode spectrum. The fitted background is then subtracted. The resulting residuals in power spec-
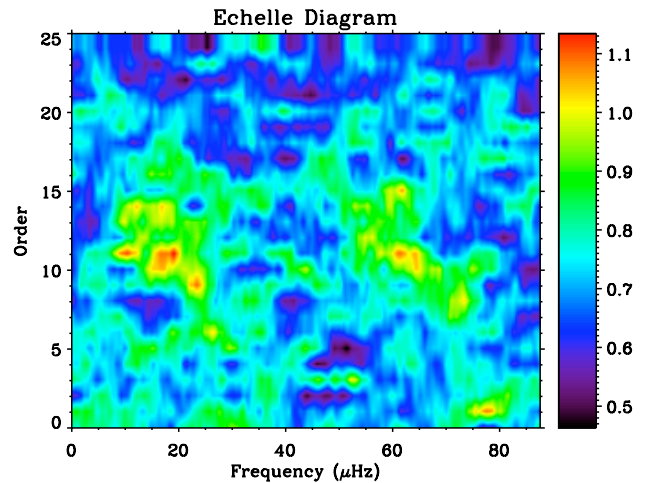
tral density will be greater than zero over ranges occupied by significant mode power.

Re-calibration of the residual averages then allows for an estimate of the equivalent $l = 0$ mode amplitudes (Kjeldsen et al. 2008). To re-calibrate, one must: (i) multiply by $q\Delta\nu$, to give the average *power* across frequency intervals of this length; and (ii) normalize to power per $l = 0$ mode, by dividing by qV_{tot}, where V_{tot} is the combined visibility of the $l = 0, 1, 2$ and 3 modes (again, see Kjeldsen et al. (2008)).

In practice we ran a boxcar of width $q\Delta\nu$ through the spectrum in order to better estimate the maximum power (one could miss the true maximum if the independent slices cut through pairs of modes). The measured maximum mode rms amplitude was $A_{max} = 2.9 \pm 0.3$ ppm.

We also applied a different approach to estimation of the amplitudes. This approach assumed the envelope of excess power due to the modes could be modelled by a Gaussian function. We fitted a Gaussian profile to the re-calibrated residual averages (see above), and from the best-fitting maximum we estimated $A_{max} = 2.8 \pm 0.1$ ppm. The location in frequency of maximum also allowed us to estimate the frequency of maximum power, which was $\nu_{max} = 1912 \pm 47\,\mu$Hz.

To convert these instrumental values into maximum intrinsic bolometric amplitudes per radial mode, $A_{bol}(l = 0)$, we took into account the instrumental response functions for CoRoT, as presented by (Michel et al. 2009). We then found that $A_{bol}(l = 0) = 3.26 \pm 0.42$ ppm (Michel et al. 2008a). This amplitude is about one third smaller than the expected value deduced from the scaling laws. Such a deficit is also seen for the other hot, solar-like oscillators observed by CoRoT (Michel et al. 2008a). HD 181906 is not significantly undermetallic, so it is hard to appeal to a metallicity effect as a possible explanation (e.g., as in Mosser et al. (2008)). However, we note that this star – like the other solar-like CoRoT targets HD 49933, HD 175726, and HD 181420 – rotates significantly faster than the Sun (10 times for this target) and exhibits clear magnetic activity (cf. Sect. 4). It could be an indication that the magnetic activity plays a role in suppressing the p-mode amplitudes by changing the surface convection and thus modifying the efficiency of p-mode excitation processes. Some 3D compressible radiative magnetohy-

drodynamics simulations (Jacoutot et al. 2008) have shown such effects.

There is another possibility, which is that the discrepancy could be explained by a blending effect. Bruntt (2009) have shown evidence in the spectrum of HD 181906 for the superimposition of a second spectrum, which could be a companion or a star in the background field. If this is the case, the relative amplitudes of modes could easily be underestimated by a factor of 1.5, making them compatible with the observations.

7.2. The mean large separation

Different methods have been used for extracting the large separation of the p-mode spectrum. A good signature of this large separation can be derived from the PSPS, or from the autocorrelation of the power spectrum, computed in the region where the excess of power has been detected (see Fig. 9).

Taking the frequency interval where the p-mode excess has been found (see Sect. 5), i.e. from 1400 to 2100 μHz, we find that the PSPS is dominated by a peak at 6.35 hours (see Fig. 7), which corresponds to half the large separation of 43.75 μHz. Indeed, the main periodicity we found is not the large separation itself but the distance between peaks of even and odd degree. Therefore, the large separation is $\Delta\nu = 87.5 \pm 2.6$ μHz (see Fig. 7). Depending on the range in frequency used to look for the large separation, different groups have found slightly different values. For example, if we reduce the search range to 1400 to 2000 μHz, the large separation is reduced to a value of 85.7 ± 2.6 μHz.

Another powerful way to estimate the value of the large separation is to build the so-called collapsogram (Korzennik 2008). The first step consists in calculating all the Echelle diagrams for a frequency range in which we expect the large separation (e.g. 60-100 μHz). The second step then consists in collapsing the vertical dimension of each Echelle diagram. In the last step the collapsed diagrams are stacked vertically, to yield the final collapsogram.

The collapsogram presents two advantages. First, it allows us to explore on a single diagram a wide range of possible values of the large separation. Secondly, it increases the visibility of the separation compared to that seen in the Echelle diagram (although it does rely on the separation being almost uniform over the frequency range used to construct the collapsogram).

In Fig. 11, we present the collapsogram of the smoothed power spectrum obtained with a weighted moving average over 11 bins. The presence of the two mode ridges is seen, with the large separation indicated as being between 85 to 90 μHz. Note that we have considered only the power spectrum in the frequency range between 1300 and 2300 μHz to build the collapsogram.

7.3. Comparison with other observed F stars

A comparison of published global parameters (and their associated error bars when available) from different F stars is presented in Table 3 where $\Delta\nu$ is the large spacing, ν_{max} is the frequency in the spectrum with the maximum power and A_{max} is the bolometric maximum amplitude per radial mode. In the case of Procyon, the bolometric amplitude is obtained from the velocity measurements following Arentoft et al. (2008). The stars HD 181906, HD 49933, HD 181420 and HD 175726 are observed by CoRoT. However, the length of observations is not the same for all of them, being 156 days for HD 181906 (the star
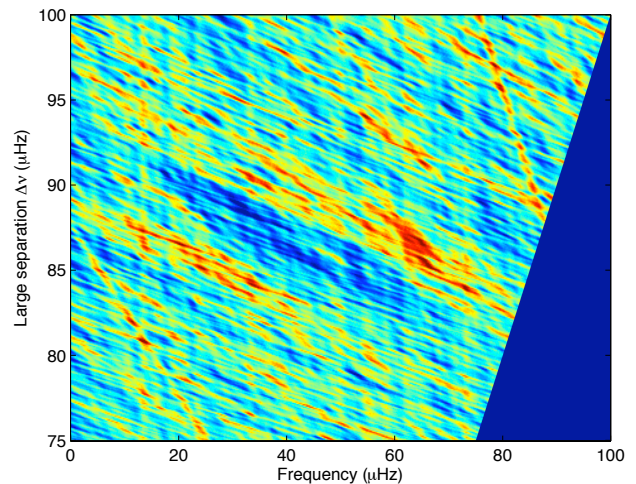

Fig. 11. Collapsogram of the smoothed power spectrum (11 bins) obtained by collapsing the power spectrum in the frequency range between 1280 and 2300 μHz. The vertical axis corresponds to the large separation that was explored, i.e., from 75 to 100 μHz. The horizontal axis indicates the frequency, from 0 to 100 μHz, which is the maximum large separation that was looked for. Note that there are two prominent excesses of power in the collapsogram, corresponding to a large separation of about 85 to 90 μHz, at $\simeq$27 and $\simeq$67 μHz.

analyzed in this paper) and HD 181420 (Barban et al. 2009), 60 days for HD 49933 (Appourchaux et al. 2008) and only 27 days for HD 175726 (Mosser et al. 2009b). The data from Procyon correspond to velocity measurements obtained during 26 days for a multisite campaign involving 11 telescopes (Arentoft et al. 2008).

The data in Table 3 are obtained mainly from the above mentioned papers, except the bolometric maximum amplitude per radial mode (A_{max}) for the 3 first mentioned CoRoT stars that were obtained from Michel et al. (2008a). For Procyon, the T_{eff}, $v \sin i$, and [Fe/H] were obtained from Allende Prieto et al. (2002). The value of the maximum amplitude in the spectrum is a translation from cm/s to ppm done in Arentoft et al. (2008) by the authors, a value that agrees well with the one obtained by Bruntt et al. (2005) using white-light photometric data from the WIRE satellite.

8. Extracting individual p-mode characteristics

Although fitting low-degree p-mode profiles in helioseismology and asteroseismology might appear very similar, the unknown stellar inclination angle makes the fitting of asteroseismic data much more difficult (see for example Appourchaux et al. (2008) for the case of the star HD 49933 or Gizon & Solanki (2003) for Monte-Carlo simulations with artificial p-mode profiles). It is not only the lower signal-to-noise ratio of the p-mode asteroseismic signal which makes the fitting difficult but also the high correlation between the inclination and the rotational splitting (Ballot et al. 2006, 2008). Because of that, the determination of these two parameters can be rather poor and will consequently affect the determination of the other parameters (frequencies, widths, heights...). Therefore, instead of fitting individually each multiplet or pair of modes – as it is commonly done in helioseismology – we choose to perform a global fitting of all the

**Table 3.** Comparison of published global parameters for different F stars.

Stars	HD181906 This paper	HD49933 Appourchaux et al. 2008	HD181420 Barban et al. 2009	HD175726 Mosser et al. 2009b	Procyon Arentoft et al. 2008
Spectral Type	F8	F5	F2	F9/G0	F5
T_{eff}	6300 ± 150 K	6780 ± 130 K	6580 ± 105 K	6000 ± 100 K	6514 ± 27 K
[Fe/H]	-0.11 ± 0.14 dex	-0.37 dex	0.00 ± 0.06 dex	-0.22 ± 0.1 dex	-0.05 dex
$v \sin i$	10 ± 1 km s^{-1}	$9.5 - 10.9$ km s^{-1}	18 ± 1 km s^{-1}	13.5 ± 0.5 km s^{-1}	3.16 ± 0.5 km s^{-1}
$\Delta\nu$	87.5 ± 2.6 μHz	85.9 ± 0.15 μHz	~ 75 μHz	$\sim 97\mu$Hz	~ 55 μHz
ν_{max}	1900 μHz	1760 μHz	1500 μHz	2000 μHz	900 μHz
A_{max}	3.26 ± 0.42 ppm	4.02 ± 0.57 ppm	3.82 ± 0.40 ppm	~ 1.7 ppm	~ 8.5 ppm

multiplets above a given amplitude threshold around the maximum of the p-mode hump, assuming that the rotational splitting is independent of the frequency (see Appourchaux et al. 2008, for all the details). This type of global method was pioneered by Roca Cortés et al. (1999) using solar data. By doing so, the splitting and the inclination angle are better constrained, even though HD 181906 is then modeled as a rigidly rotating star. Each multiplet is described by five parameters: the central frequencies of the modes $l = 0, 1, 2$, one line width (the same for all modes within a large separation), and one mode height. We assumed the same visibility ratio between angular degrees as the ones used in full-disk helioseismology and the visibilities between m-components given by Gizon & Solanki (2003).

Eight teams performed a global fitting of the HD 181906 data, seven of them using a maximum likelihood minimization and one using a least square fitting over an averaged spectrum. All the teams did the fits for both scenarios (A and B) depending on the identification of the ridges as the odd or even modes.

Two teams decided to split the observations in four subseries and computed the Joint Power Statistics (JPS, see Appendix A for a detailed explanation). The JPS is an alternative method that contains the same underlying information as the average spectrum but with a different treatment of the noise. The rest of the teams worked on the full resolution power spectrum. The number of overtones fitted was 5, 7, 9 and 16 overtones. Different strategies have also been followed by each team to obtain the initial parameters for the fit. In particular, one team used the results from HD 49933 (Appourchaux et al. 2008) as a guideline since their PSDs look very similar and HD 49933 has a much better signal-to-noise ratio. Figure 12 shows the superposition of the PSD of HD 181906 and the one of HD 49933 – properly scaled in amplitude – and shifted by 17 μHz. Thus, the initial guesses were obtained directly from the fitted values of HD 49933. Another team repeated the fits 200 times for each scenario, adding scatter to the initial parameters in order to test the robustness of the fits and identify any correlation between the initial seed values and the fitted ones. As expected, the inclination angle was identified to be strongly correlated with the initial seed angle.

The mode parameters were then extracted using different approaches based on the recipe developed by the Data Analysis Team (DAT) and explained in Appourchaux et al. (2008). However, in order to have a more reliable characterization of the p-mode signal, given the low signal-to-noise ratio of the observations, some more a-priori information needed to be introduced. In order to stabilize the fits and avoid systematic outliers, some of the fitting teams fixed some parameters to be equal over the range of considered overtones. For instance, without some a-priori conditions, the minimization procedures failed to return reliable estimates at high frequency, fitting mostly spikes and over-estimated heights. Tables 4 and 5 show the fitted mode
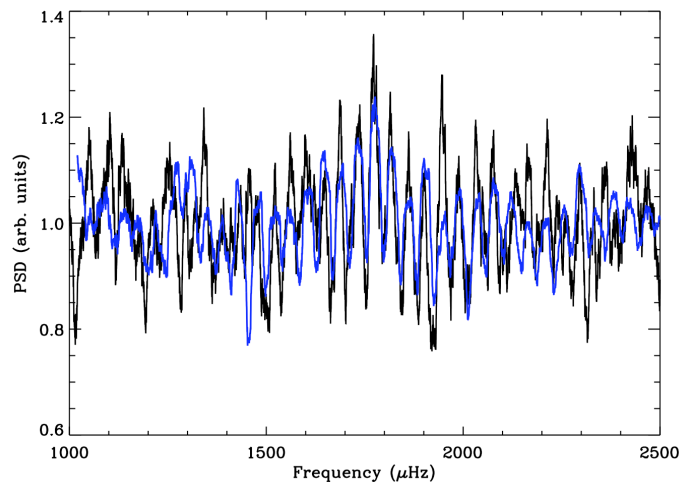
Fig. 12. Smoothed power spectrum of HD 181906 (black curve) and smoothed and shifted by 17 μHz power spectrum of HD 49933 (blue curve).

frequencies obtained from the less constrained fit for both scenarios A and B respectively, the analysis being performed on the power spectrum of the whole HD 181906 time series. The only condition applied to those fits is that the mode widths and mode heights were set to be uniform (the same for all the modes) over the fitted frequency range. In the central part of the p-mode hump, those frequency estimates are consistent within 3σ with the estimates returned using more constrained fits and different dataset lengths. In the low- and high-frequency ranges, the discrepancies are larger but still within 5σ. Unfortunately, neither of the scenarios seems to be favoured: for instance, the likelihood ratio test does not allow us to disentangle between the two possibilities, the likelihood ratio being not greater than 5 (for the fits presented here).

Table 4. HD 181906 frequencies (in μHz) for scenario A.

	Scenario A		
#	$l = 0$	$l = 1$	$l = 2$
1	1524.80 ± 0.86	1565.61 ± 0.38	1521.98 ± 0.42
2	1604.89 ± 0.25	1645.98 ± 0.41	1596.46 ± 0.51
3	1684.62 ± 0.40	1734.98 ± 0.53	1687.32 ± 0.51
4	1773.14 ± 0.27	1814.29 ± 0.31	1772.43 ± 0.39
5	1862.25 ± 0.53	1898.77 ± 0.27	1861.74 ± 0.39
6	1947.42 ± 0.30	1988.32 ± 0.37	1946.26 ± 0.28
7	2035.88 ± 0.62	2076.45 ± 0.51	2036.30 ± 0.95

Table 5. HD 181906 frequencies (in μHz) for scenario B.

	Scenario B		
#	$l = 0$	$l = 1$	$l = 2$
1	1565.96 ± 0.38	1521.94 ± 0.41	1560.55 ± 0.65
2	1646.63 ± 0.35	1604.76 ± 0.29	1644.97 ± 0.41
3	1734.59 ± 0.26	1684.74 ± 0.62	1735.54 ± 0.53
4	1814.83 ± 0.41	1772.68 ± 0.27	1814.16 ± 0.41
5	1898.79 ± 0.43	1861.91 ± 0.43	1898.46 ± 0.40
6	1988.50 ± 0.33	1947.04 ± 0.25	1988.72 ± 0.44
7	2075.91 ± 0.32	2036.48 ± 0.69	2077.20 ± 0.38

Nevertheless, we can still obtain some global characteristics of HD 181906. On one hand, the fitted inclination angle, for both scenarios (around $47^{\rm o} \pm 3.5^{\rm o}$) , is very close to the one derived from the analysis of the low-frequency peak of the PSD (see Sect. 4) when a $(v \sin i)_{obs} \approx 16 \pm 1$ km s^{-1} is considered but quite far from the $\sim 24^{\rm o}$ obtained considering $(v \sin i)_{obs} \approx 10$ km s^{-1}. On the other hand, the extracted rotational splitting (5.8 and 6.1 ± 0.14 μHz respectively for A and B scenarios) is overestimated compared to the surface rotation rate (see Sect. 4). This could be due to an increase of the rotation rate in the stellar interior or a biased estimation due to the a-priori conditions applied to the fit (a common height and width for all the fitted modes).These results show, once again, the strong correlation between these two parameters and the necessity to have an external good determination of the inclination angle or the rotation of the star to be able to disentangle between the possible solutions.

Another parameter – the global line width – was found to be rather small (1.25 -0.3/+0.4 and 1.28 -04/+0.6 μHz for scenarios A and B respectively), which is probably a consequence of the low SNR that could bias this estimate when we apply our peak-bagging codes: the low SNR means the modes will appear "spikier" than they really are (we lose the Lorentzian tails in the background noise), meaning we will be biased to fitting small line widths. We expect that the autocorrelation of the power spectrum will have better SNR than that seen in individual modes and hence we look there for the features associated with mode line width. The features in it are quite wide, implying that the line widths are large and probably in line with what we saw for HD 49933 (see Fig. 12). Indeed, the widths of the modes in both stars, around the maximum of the p-mode spectrum, seem to be similar which favours shorter mode lifetimes than in the Sun.

Finally, we would like to emphasize that the combination of a small SNR, a possible small inclination angle of the star (close to 25°) and large mode line widths produce similar Lorentzian profiles for the modes l=0, 2 and 1 (Ballot et al. 2004). This effect could contribute to explaining why we obtain very similar fitting results in both scenarios. More work will be necessary to obtain more reliable individual p-mode parameters.

9. Conclusion and perspectives

In this paper we have shown the first seismic analysis of HD 181906 (HIP 95221), a faint CoRoT target (m_v=7.65) that has been observed continuously during 156.6 days in 2007. The surface rotation of the star has been inferred by analyzing the very low-frequency part of the power spectrum. A rotation rate of 2.9 days (4 μHz) has been established. The presence of a second peak close to the previous one in the power spectrum and produced during a different period of time, has been interpreted as the signature of the presence of magnetic structures on the stellar surface at different latitudes and, therefore, it has been deduced that this star could have a slightly higher differential rotation than the Sun. Coupling this rotation rate with the previous result of the $(v \sin i)_{obs} \approx 16 \pm 1$ km s^{-1} has allowed us to infer an inclination angle of $37.5^{\rm o} \pm 4.5^{\rm o}$ but this value could be reduced to $24^{\rm o} \pm 3^{\rm o}$ if we consider that HD 181906 has a companion which implies a reduction in the $(v \sin i)_{obs}$ to 10 ± 1 km s^{-1}.

A comb-like structure has been unveiled between 1400 and 2100 μHz which corresponds to the acoustic-mode spectrum with a maximum power at 1912 ± 47 μHz and a large separation of 87.5 ± 2.6 μHz measured inside this frequency interval. However, the low signal-to-noise ratio of the modes prevents us from unambiguously identifying them. To go further, more a-priori information is needed to constrain the fits.

References

Allende Prieto, C., Asplund, M., López, R. J. G., & Lambert, D. L. 2002, ApJ, 567, 544
Appourchaux, T. 2004, A&A, 428, 1039
Appourchaux, T., Michel, E., Auvergne, M., et al. 2008, A&A, 488, 705
Arentoft, T., Kjeldsen, H., Bedding, T. R., et al. 2008, ApJ, 687, 1180
Auvergne, M., Bodin, P., Boisnard, L., et al. 2009, ArXiv e-prints 0901.2206
Baglin, A., Auvergne, M., Boisnard, L., et al. 2006, in COSPAR, Plenary Meeting, Vol. 36, 36th COSPAR Scientific Assembly, 3749–+
Ballot, J., Appourchaux, T., Toutain, T., & Guittet, M. 2008, A&A, 486, 867
Ballot, J., García, R. A., & Lambert, P. 2006, MNRAS, 369, 1281
Ballot, J., García, R. A., Lambert, P., & Teste, A. 2004, in ESA Special Publication, Vol. 559, SOHO 14 Helio- and Asteroseismology: Towards a Golden Future, ed. D. Danesy, 309–+
Barban, C., Deheuvels, S., Baudin, F., et al. 2009, A&A, This volume
Bedding, T. R. & Kjeldsen, H. 2003, Publications of the Astronomical Society of Australia, 20, 203
Bruntt, H. 2009, A&A, submitted
Bruntt, H., Kjeldsen, H., Buzasi, D. L., & Bedding, T. R. 2005, ApJ, 633, 440
Chaplin, W. J., Appourchaux, T., Arentoft, T., et al. 2008, Astronomische Nachrichten, 329, 549
Chaplin, W. J., Elsworth, Y., Isaak, G. R., et al. 2002, MNRAS, 336, 979
Frankowski, A., Jancart, S., & Jorissen, A. 2007, A&A, 464, 377
García, R. A., Appourchaux, T., Baglin, A., et al. 2008, Communications in Asteroseismology, 157, 288
Gizon, L. & Solanki, S. K. 2003, ApJ, 589, 1009
Goupillaud, P., Grossmann, A., & Morlet, J. 1984, Geoexploration, 23, 85
Grec, G., Fossat, E., & Pomerantz, M. A. 1983, Sol. Phys., 82, 55
Holmberg, J., Nordström, B., & Andersen, J. 2007, A&A, 475, 519
Jacoutot, L., Kosovichev, A. G., Wray, A., & Mansour, N. N. 2008, ApJ, 684, L51
Kjeldsen, H. & Bedding, T. R. 1995, A&A, 293, 87
Kjeldsen, H., Bedding, T. R., Arentoft, T., et al. 2008, ApJ, 682, 1370
Korzennik, S. G. 2008, Advances in Space Research, 41, 897
Makarov, V. V. & Kaplan, G. H. 2005, AJ, 129, 2420
Masana, E., Jordi, C., & Ribas, I. 2006, A&A, 450, 735
Mathur, S., Jimenez-Reyes, S. J., & Garcia, R. A. 2008, in Proceedings of GONG 2008/SOHO XXI, Solar-stellar dynamos as revealed by helio- and asteroseismology
Michel, E., Baglin, A., Auvergne, M., et al. 2008a, Science, 322, 558
Michel, E., Baglin, A., Weiss, W. W., et al. 2008b, Communications in Asteroseismology, 156, 73
Michel, E., Samadi, R., Baudin, F., et al. 2009, A&A, 495, 979
Mosser, B., Baudin, F., & Lanza, A. 2009a, A&A, This volume
Mosser, B., Deheuvels, S., Michel, E., et al. 2008, A&A, 488, 635

Mosser, B., Roxbourgh, I., Michel, E., et al. 2009b, A&A, This Volume

Nordström, B., Mayor, M., Andersen, J., et al. 2004, A&A, 418, 989

Press, W. H., Teukolsky, S. A., Vetterling, W. T., & Flannery, B. P. 1992, Numerical recipes in FORTRAN. The art of scientific computing (Cambridge: University Press, —c1992, 2nd ed.)

Roca Cortés, T., Jiménez, A., Pallé, P. L., GOLF team, & VIRGO Team. 1999, in ESA Special Publication, Vol. 448, Magnetic Fields and Solar Processes, ed. A. Wilson & et al., 135–+

Samadi, R., Fialho, F., Costa, J. E. S., et al. 2007a, ArXiv Astrophysics e-prints

Samadi, R., Georgobiani, D., Trampedach, R., et al. 2007b, A&A, 463, 297

Sturrock, P. A., Scargle, J. D., Walther, G., & Wheatland, M. S. 2005, Sol. Phys., 227, 137

Torrence, C. & Compo, G. P. 1998, Bulletin of the American Meteorological Society, 79, 61

van Leeuwen, F. 2007, A&A, 474, 653

Appendix A: Joint Power Statistic

In cases where the signal-to-noise ratio of a power spectrum is low, it can be useful to increase the signal and decrease the noise at a cost of decreasing the resolution in frequency. This has often been accomplished by calculating either the arithmetic or geometric mean of a set of power spectra obtained from independent contiguous subsets of the complete time series. The expected statistics of these averaged power spectra can be calculated, however they do not have the same negative exponential distribution as a single power spectrum. The standard maximum likelihood estimation (MLE) fitting techniques are designed for power spectra with negative exponential statistics (*i.e.* χ^2 with 2 d.o.f.), it is therefore desirable to calculate an averaged power spectrum with the same statistics as the original spectrum.

The joint power statistic (JPS) (Sturrock et al. 2005) esembles a correlation function in the sense that it increases the contribution of signals present in a number of independent power spectra while decreasing the uncorrelated noise. It also has the important property that the JPS is distributed with negative exponential statistics and can, therefore, be immediately fitted using established MLE techniques. The JPS can be calculated using the power spectra of any number of independent subseries, with the resolution in frequency decreasing by a proportional amount compared with the power spectrum of the complete time series. In the case of HD 181906, the best compromise between increasing the amplitude-to-background ratio and maintaining sufficient resolution in frequency was found when the complete detrended time series was divided into four contiguous subseries. The appropriate fourth order JPS can be approximated by

$$J_{4A} = \frac{3.881X^2}{1.269 + X}, \tag{A.1}$$

where X is the geometric mean of the power spectra (S_i) calculated from four independent subseries

$$X = (S_1 S_2 S_3 S_4)^{1/4}. \tag{A.2}$$

In the JPS calculated from four subseries, after smoothing with a Gaussian filter of width $1\sigma = 2\,\mu$Hz, the average amplitude-to-background ratio for mode peaks between 1700 and 2000 μHz is 2.8. This compares with the equivalent full series smoothed FFT amplitude-to-background ratio of 1.7 over the same range. While the JPS can be fitted assuming negative exponential statistics, the mode amplitudes obtained will be higher than those obtained from a single power spectrum due to the increase in power of correlated signals in the JPS. Similarly, the stellar background parameters obtained from a JPS fit will be lower than those obtained from a power spectrum fit. The mode frequencies and linewidths obtained from the JPS are the only parameters that are directly comparable with a fit to the power spectrum.